miRNA-101 Regulates Filamentogenesis During Migration and Invasion of Cervical Cancer Cells

Ping Zhang
Xinjiang Medical University
Muli Wudu
Xinjiang Medical University
Zi-Qi Huang
Xinjiang Medical University
Yang Liu
Xinjiang Medical University
Abuliaizezi Erken
Xinjiang Medical University
Chen Lin (linmao1977@126.com)
Xinjiang Medical University https://orcid.org/0000-0001-6880-4927

Primary research

Keywords: cervical cancer, filopodia, invasion, microRNA-101, migration.

Posted Date: August 11th, 2020

DOI: https://doi.org/10.21203/rs.3.rs-55338/v1

Abstract

Background: miRNAs play critical roles in cervical cancer (CC) progression. miRNA-101 is a tumour suppressor in several cancers. The aim of this study was to investigate the *in vitro* and *in vivo* effect of miRNA-101 on the biological behaviour of CC cells by analysing the formation of filamentous pseudopodia.

Methods: Quantitative reverse-transcription-polymerase chain reaction was performed to analyse miRNA-101 expression in CC cells before and after its transfection. Cell counting kit-8, transwell migration, and wound healing assays were performed to investigate the effect of miRNA-101 on the malignant behaviour of CC cells *in vitro*. The impact of miRNA-101 on filopodia initiation in CC cells was investigated via scanning electron microscopy and TRITC-labelled phalloidin staining evaluation. *In vivo* analysis was performed using a nude mouse model of CC, established via subcutaneous tumour transplantation, to validate the role of miRNA-101 on CC malignant behaviour. One-way ANOVA with Fisher's least significant difference post hoc test and *t*-test were used to evaluate statistical significance of differences between groups.

Results: miRNA-101 was significantly downregulated in CC cell lines. Overexpression of miRNA-101 inhibited the malignant behaviours of CC cells *in vitro*, while it inhibited the formation of filopodia in CC cells. Similar results were observed using immunofluorescence and confocal microscopy.

Conclusions: These results indicate that miRNA-101 inhibits CC migration and invasion. The present findings, combined with future research, will help provide a theoretical basis and novel insight for the clinical management of CC.

Background

Cervical cancer (CC) is one of the most common malignancies in women worldwide. In 2012, 527,000 new cases and 265,700 CC-related deaths were reported [1, 2]. In recent years, owing to the use of various diagnostic screening methods and surgical procedures, the incidence of CC showed a decreasing trend [3]; however, it remains the primary cause of mortality among women. The incidence of CC is particularly high among Uyghur women in the Xinjiang Uygur Autonomous Region of China, where most patients have advanced CC with a high mortality rate [4]. Metastasis, especially to the pelvic lymph node, is a major pathognomonic hallmark of CC that is associated with poor prognosis and high mortality. Therefore, the early detection of metastasis and relapse, as well as improvement of prognosis, are critical for CC outcome.

Some recent studies have reported that the rearrangement of cytoskeleton proteins forms the cellular basis of tumour adaptation to new environments and their migration [5]. Changes in cytoskeletal morphology prominently influence tumour motility, permeability, and angiogenesis, potentially causing tumour cells to invade the surrounding tissues and gradually develop distant metastasis. Filopodia,

located at the anterior region of the cell, guides the posterior region of the cell to move forward and serves as a ‘sensory organ’ for communication with the extracellular microenvironment.

miRNAs are non-coding single-stranded RNAs of 18–24 nucleotides [6] that contribute to the regulation of tumorigenesis and tumour behaviour in humans [7]. We previously reported 12 differentially expressed miRNAs (all down-regulated) in CC tissues derived from Uyghur women, wherein miRNA-101 was down-regulated more than 3-fold and was associated with lymph node metastasis in CC. miRNA-101 was significantly down-regulated in HeLa and SiHa CC cell lines, and its up-regulation inhibited CC cell invasion [8, 9].

The aim of this study was to: (1) construct a lentiviral vector harbouring miRNA-101 to infect CC cell lines, (2) observe filamentogenesis in CC cells via scanning electron microscopy (SEM) and TRITC-labelled phalloidin staining, (3) perform scratch healing, transwell, and matrigel assays to examine CC cell invasion and migration, and (4) establish a mouse model of CC lung metastasis using BALB/c nude mice and investigate the effect of miRNA-101 on subcutaneously transplanted CC cell lines in the nude mice.

Materials And Methods

Cell lines and cell culture protocols

The human CC cells lines HeLa and SiHa were purchased from the Cell Culture Collection of the Shanghai Branch of the Chinese Academy of Sciences. HeLa and SiHa cells were cultured at 37 °C and 5% CO_2 in Dulbecco's Modified Eagle Medium (Gibco, Waltham, MA, USA) supplemented with 10% foetal bovine serum (Gibco) and 2% penicillin–streptomycin (Beyotime Biotechnology, Haimen, China). On approaching 80%–90% confluence, cells were trypsinised.

Construction, packaging, and transduction of lentiviral vectors

Lentivirus GV-miRNA-101 (Genechem, Shanghai, China) was used to infect SiHa and HeLa cells at a multiplicity of infection (MOI) of 10 and lentivirus GV-EGFP (Genechem) was used as the control vector. After 72 h of transduction, cells were harvested and used for subsequent tests.

RNA isolation and quantitative reverse-transcription-polymerase chain reaction (qRT-PCR)

Total RNA was isolated using Trizol reagent (Invitrogen, Carlsbad, CA, USA) and 1 μg of total RNA was retrieved using the miScript RT Kit (Qiagen, Hilden, Germany). The Bio-Rad CFX96 system (Hercules, CA, USA) with miScript SYBR Green (Qiagen) was used for qRT-PCR analysis and to determine the expression levels of the *mRNA-101* and genes of interest. The qRT-PCR protocol was as follows: 95 °C for 15 min, followed by 40 cycles at 94 °C for 15 s, 55 °C for 30 s, and 70 °C for 30 s. After 40 amplification cycles, the melting curve was examined, the Ct value of each sample was automatically calculated, and relative mRNA expression levels were determined using the $2^{-\Delta\Delta CT}$ algorithm. The samples were analysed in triplicate and *U6* was used as an internal control for miRNA amplification. *miRNA-101* and *U6* were

reverse-transcribed (RT) with Bulge-loop miRNA qRT-PCR primers (one pair of RT primers and one pair of qPCR primers in each group) designed by Ribo Bio (Guangzhou, China).

Cell counting kit (CCK)-8 assay

The lentivirus-transduced CC cells were seeded in 96-well plates at 5×10^3 cells/well and cultured overnight at 37 °C and 5% CO_2. Thereafter, 10 μL of CCK-8 solution was added into each well and incubated for 24, 48, and 72 h and the absorbance was measured at 450 nm, using a microplate reader (Bio-Rad). The control group comprised human CC cells transduced with a sham lentivirus. Cell viability was determined using the formula: cell viability = (absorbance of the test well - absorbance of the blank well)/(absorbance of the control well - absorbance of the blank well) × 100%.

Scanning electron microscopy (SEM) analysis

The same number of cells (HeLa and SiHa) was seeded on a glass coverslip (0.8×0.8 cm^2), placed in a 48 well plate, and cultured in Dulbecco's Modified Eagle Medium at 37 °C and 5% CO_2. When the cell fusion rate approached 50%, the coverslips were removed, fixed with 3.7% formaldehyde for 10 min, and washed thrice with phosphate-buffered saline (PBS), followed by sequential dehydration, air-drying, and placement on a short column. Thereafter, the slides were placed in the vacuum chamber of an SEM gold coating apparatus (plating instrument) and gold-coated at 2.5 kV, 20–25 mA for 2 min. The cells were then observed using a SEM (JEOL JSM-5800, Japan) at an accelerating voltage of 20 kV.

Immunofluorescence and confocal microscopic assays

CC cell lines (2×10^4 cells) were inoculated on a confocal plate and examined 24 h later. Cells were then fixed with 4% formaldehyde, stained with TRITC-labelled phalloidin (1:100; Solarbio, Beijing, China) at 25 °C for 30 min, followed by staining with DAPI (Solarbio) at 25 °C for 30 s. Images were acquired using the FV1000 confocal microscope (Olympus, Tokyo, Japan).

Wound healing assay

The wound healing assay was performed to evaluate the migration potential of CC cells. Briefly, human CC cell lines were inoculated onto 6-well plates (1×10^6 cells/well). Upon 70%–80% cell fusion, artificial wounds with the same width were obtained by scratching the the cell layer with sterile plastic micropipette tips. Thereafter, cell debris were eliminated by washing with PBS. Cell migration was observed and photographed at 24, 48, and 72 h after wounding and compared with the 0 h image.

Combinatorial transwell and matrigel assay

Cell invasion was assessed using matrigel invasion chambers (BD Bioscience, San Diego, CA, USA). Briefly, 3×10^4 cells were seeded in serum-free medium in the upper chamber. The medium, supplemented with 10% foetal bovine serum, was added to the lower chamber. After 24 h of culturing, the cells at the

bottom of the membrane were fixed and stained with 0.1% crystal violet. Five visual fields of invasive cells were randomly selected, counted, and photographed under a microscope.

Xenograft mouse model of CC

All procedures involving mice were approved by the Experimental Animal Ethics Committee of Xinjiang Medical University and met all regulatory standards. Forty-five female (4–6 weeks old) BALB/c nude mice were divided into three groups (n = 15/group). A 0.2 mL cell suspension (5×10^6 cells) was subcutaneously injected into the right forelimb capsule. The blank group comprised mice injected with HeLa cells, the control group comprised mice injected with HeLa cells transfected with empty-load lentivirus, and the experimental group comprised mice injected with HeLa cells transfected with miRNA-101 lentivirus. The physiological features (including mental state, activity, diet, body weight, appearance, and tactile responses to touching the inoculated area) of nude mice were evaluated every 2–3 days. Tumour growth (characterised by the number of subcutaneous xenografts, the long diameter [L], and short diameter [W] of the subcutaneous xenografts that were measured with a Vernier calliper, and tumour volume [V, mm^3]), was determined using the following formula: $V = (L \bullet W^2)/2$. After 39 days of cell inoculation and when the diameter of the subcutaneous xenografts approached approximately 9 mm, the nude mice were euthanized and the tumour tissue was excised. The growth curve of the subcutaneous xenografts was constructed on the basis of V and inhibition rate (in %), which was determined as inhibition rate = (1 − [(average initial V of the experimental group − average final V of the experimental group)/(average initial V of the control group − the average final V of the control group)]) × 100%.

Histopathological analysis

Tumour, lung, liver, heart, kidney, and brain tissues were fixed with normal neutral formalin, embedded in paraffin, sectioned, stained with haematoxylin and eosin, and the histological characteristics of the transplanted tumour and critical organs were observed using a light microscope.

Statistical analyses

The experimental data were analysed using SPSS19.0 software (IBM Inc, Armonk, NY, USA) and all graphs were plotted using GraphPad Prism for Windows version 5.0 (GraphPad Software, San Diego, CA, USA). Continuous variables were expressed as mean ± standard deviation values and the data were assessed for normality and conformance with a normal distribution. The one-way ANOVA was performed to compare the homogeneity of the assessed differences among groups and independent samples *t*-test was used for between-group comparisons. Each experiment was performed in triplicate. A *P*-value < 0.05 was considered statistically significant. Tumour volume among groups was simultaneously analysed using a one-way ANOVA and Fisher's least significant difference test (variance uniformity) for post hoc pairwise comparison.

Results

Efficiency of miRNA-101 lentiviral transduction in CC cells

The miRNA-101 lentiviral vector was used to infect HeLa and SiHa cells. After 48–72 h of infection, fluorescence expression was observed with a laser-scanning confocal microscope to determine the transduction efficiency, as the GFP-encoding gene was incorporated into the lentiviral vector to produce green fluorescence after CC cell infection. MOI values of the miRNA-NC group (infected with the control fluorescent lentiviral vector) and miRNA-101 group (infected with the lentiviral vector harbouring miRNA-101) were screened via laser-scanning confocal microscopy. At an MOI of 10, the fluorescence abundance of HeLa and SiHa cells in both groups was > 80%. After sub-culturing, HeLa and SiHa cells in the two groups displayed non-significant fluorescence attenuation. At an MOI of 10, the lentivirus stably transfected CC cells and subsequent experiments were conducted.

miRNA-101 overexpression inhibits the growth and proliferation of CC cells

To further investigate the effect of miRNA-101 on human CC cells, we performed functional assays using CC cells overexpressing miRNA-101. qRT-PCR analysis revealed that after transduction, *miRNA-101* was significantly up-regulated ($P < 0.05$) in CC cells compared to miRNA-NC transfected cells (Fig. 1a, b), whereas it was not significantly expressed ($P > 0.05$) in the untreated group and miRNA-NC group. The CCK-8 assay revealed that miRNA-101 overexpression significantly decreased the viability and proliferation ($P < 0.05$) of Hela cells (Fig. 1c). Similarly, miRNA-101 forced expression in SiHa cells inhibited cell proliferation compared to the control group (Fig. 1d).

miRNA-101 overexpression inhibits CC cell migration and invasion

We performed the wound healing and combinatorial transwell and matrigel assays to examine the effect of miRNA-101 on CC cell migration and invasion. The wound healing rate of miRNA-101-overexpressing cells was significantly lower ($P < 0.05$) than that of the normal control group, and no difference was observed between the miRNA-101-untreated group and the normal control group (Fig. 2a, c). Similarly, miRNA-101 up-regulation markedly inhibited the invasiveness of CC cells in the combinatorial transwell and matrigel assays (Fig. 2b, d). Table 1 shows the number of miRNA-NC, miRNA-101-transfected, and untransfected HeLa and SiHa cells subjected to the migration assay.

miRNA-101 regulates filopodia initiation in CC cells

We stained and labelled cytoskeletal element F-actin with TRITC-labelled phalloidin and observed the fluorescent staining via confocal microscopy. The staining revealed that HeLa and SiHa cells had more filopodia than untransfected cells, whereas miRNA-NC-transfected HeLa and SiHa cells displayed no obvious change in the number of filopodia (Fig. 4a, b). Table 2 shows the number of filopodia in untransfected, miRNA-NS-transfected, and miRNA-101-transfected HeLa and SiHa cells. Similar results were obtained in ultrastructural analysis of the cytoskeleton via SEM (Fig. 4a, b).

miRNA-101 inhibits subcutaneous xenograft formation from CC cells in nude mice

Subcutaneous xenografts visibly developed in all three groups of nude mice and the tumorigenesis rate was 100%. The mice administered miRNA-NC-transfected and untransfected CC cells displayed a generally poor condition, with a weak mental state, limited activity, longer reaction times, and decreased water intake at later stages of the cancer, whereas those administered miRNA-101-transfected CC cells displayed a good physical and mental state, as well as adequate physical activity, and food and water intake. No significant difference was observed in body weight among the three groups of nude mice ($P > 0.05$) (Table 3).

The transplanted tumours were papillary and tough, and most had a pseudo-envelope. The transplanted tumour cells displayed low adhesion to the surrounding tissues and had a rich blood supply. In mice administered miRNA-101-transfected CC cells, some grey-white necrotic areas were observed in the centre of the transplanted tumour (Fig. 5).

Tumour volume was significantly lower in mice administered miRNA-101-transfected cells than in mice administered miRNA-NC-transfected cells ($P < 0.05$) or untransfected CC cells ($P < 0.05$). No significant difference in tumour volume was observed between mice administered miRNA-NC-transfected CC cells and those administered untransfected CC cells ($P > 0.05$) (Table 4; Fig. 6, 7).

Microscopically, tumour cells from mice administered miRNA-NC-transfected CC cells or untransfected CC cells showed an ovoid morphology and were markedly heteromorphic. The nucleus was spherical and stained purple-brown with a discernible nucleolus and the cytoplasm was unevenly stained, revealing pathological mitosis to a large extent. The tumour cells displayed marked atypia, purple-brown nuclei, discernible nucleoli, uneven cytoplasmic staining, and numerous pathological mitotic features. In mice administered miRNA-101-transfected cells, different degrees of haemorrhage and necrosis were observed at the centre of the transplanted tumour and necrotic tissue was red and granular (Fig. 8).

A comparison of the growth inhibition rates of subcutaneous xenografts in the three groups revealed that tumour growth was significantly inhibited in mice administered miRNA-101-transfected CC cells compared to mice administered miRNA-NC-transfected CC cells ($P < 0.05$) or untransfected CC cells ($P < 0.05$; Table 5).

Discussion

Numerous miRNAs are aberrantly expressed in CC and play a key role in CC pathogenesis and progression [10]. We previously reported the association between miRNA-101 down-regulation and lymph node metastasis in CC in Uyghur women in China, as well as its significant down-regulation in HeLa and SiHa cells [4]. miRNA-101 contains 21 nucleotides and is highly conserved among various species. It is down-regulated in several solid tumours including prostate, breast, lung, bladder, ovarian, and cervical cancers [11, 12]. However, studies focusing on the regulatory mechanism of miRNA-101 in different tissues have revealed inconsistent findings.

To show that miRNA-101 markedly contributes to the pathogenesis and occurrence of CC, we constructed a lentiviral vector harbouring *miRNA-101* and transfected HeLa and SiHa CC cell lines. Consequently, the proliferation potential was significantly reduced in these *miRNA-101* transfected CC cells compared to the control group, suggesting that miRNA-101 potentially inhibits the proliferation of CC cells. A previous study had showed similar results, with miRNA-101 overexpression significantly decreasing proliferation and invasion of ovarian cancer cells *in vitro* by down-regulation of SOCS-2 [13].

We performed the scratch healing test and a combinatorial transwell and matrigel assay to examine CC cell migration and invasion before and after miRNA-101 transfection. Consequently, the wound healing rate and invasiveness of miRNA-101 overexpressing cells significantly decreased, suggesting that miRNA-101 inhibits CC cell migration and invasion.

Cancer cells can use different approaches to support their migration, such as flaky pseudopodia, filamentous pseudopodia, and vesicles [14]. The formation of these processes depends on the actin cytoskeleton, which can be rapidly reconstituted and participates in the formation, movement, intracellular transport, and division of cells [15, 16]. Pseudopodium formation is the initial step of tumour cell invasion and migration. Filamentous pseudopods are usually less than 200 nm in diameter and are located at the apical end of the cell, leading the basal end of the cell to move forward [17].

Herein, SEM and TRITC-labelled phalloidin staining were performed to observe the formation of filamentous pseudopodia in CC cells transfected with the lentiviral vector harbouring miRNA-101. SEM revealed that filamentous pseudopods were amorphous filamentous processes on the cell surface, indicating that the number of filamentous pseudopods in HeLa and SiHa cells decreased significantly upon miRNA-101 transfection. Furthermore, slight differences were observed between the two cell lines. The number of amorphous processes on the surface of HeLa cells did not significantly decrease; however, the length of the processes did decreased. Therefore, this was not classified as filamentous pseudopodia. The number of amorphous processes on the surface of SiHa cells significantly decreased. Taken together, miRNA-101 overexpression inhibits the formation of filamentous pseudopods in CC cells. Four types of cells were observed upon laser-scanning confocal microscopy and TRITC-labelled phalloidin staining – polygonal/slender, non-polygonal/non-slender, unclear/early diffusion, and small spherical. Only polygonal/slender cells could be considered filamentous pseudopodia. The number of polygonal/slender cells in HeLa and SiHa CC cells significantly decreased upon transfection with the lentiviral vector harbouring microRNA-101, indicating a reduction in the number of filamentous pseudopods in HeLa and SiHa CC cells. The F-actin in filamentous pseudopodia was labelled with TRITC-labelled phalloidin, with the fluorescence intensity of different groups of cells could reflect the formation of filamentous pseudopodia at the same excitation intensity. The observed results followed the same trend as the above mentioned data on polygonal slender cells. These results indicated that miRNA-101 overexpression potentially inhibits the formation of filamentous pseudopods in CC cells, thus inhibiting migration and invasion in CC cells.

Bioinformatics analysis and pathway analyses revealed that RAC1, STMN1, and CAPN2 are associated with the regulation of the actin cytoskeleton. The Rac/WAVE/Arp2/3 pathway is essential for generating and maintaining filamentous pseudopods [18–21]. The Arp2/3 complex-mediated network stabilizes the protrusions and makes them robust [22]. However, it remains unclear whether miRNA-101 targets Rac1 in the complex pathway and affects the formation of filamentous pseudopods.

Conclusion

Altogether, these results demonstrate that miRNA-101 inhibits CC migration and invasion. Further detailed studies on the effect of miRNA-101 on filamentous pseudopodia formation, and its target genes and associated signalling pathways would elucidate the mechanism underlying invasion and metastasis in CC and provide a theoretical basis and novel insight for the clinical management of CC.

List Of Abbreviations

CC
cervical cancer
CCK
Cell counting kit
qRT-PCR
quantitative reverse-transcription-polymerase chain reaction
MOI
multiplicity of infection
PBS
phosphate-buffered saline
RT
reverse-transcription
SEM
scanning electron microscopy

Declarations

Ethics approval and consent to participate

This study was approved by the Medical Research Ethics Committee of Xinjiang Medical University (CX2018016) and informed consent was obtained from all patients.

Consent for publication

Not applicable.

Availability of data and materials

All data generated or analyzed in this study are included in this published article. Further details are available from the corresponding author upon request.

Competing interests

The authors have no competing interests to declare.

Funding

This study was supported by the National Natural Science Foundation of China (grant number 81660428).

Authors' contributions

CL and PZ conceived and designed the study. PZ, ZQH, YL, and AE performed the experiments. CL, PZ, and WW wrote the article. CL, PZ, and WW reviewed and edited the manuscript. All authors read and approved the manuscript.

Acknowledgements

We would like to thank Editage (www.editage.cn) for English-language editing.

References

1. Fang J, Li Y, Zhang J, Yan M, Li J, Bao S, et al. Correlation between polymorphisms in microRNA-regulated genes and cervical cancer susceptibility in a Xinjiang Uygur population. Oncotarget. 2017;8(19):31758–31764.
2. Niu F, Wang T, Li J, Yan M, Li D, Li B, et al. The impact of genetic variants in IL1R2 on cervical cancer risk among Uygur females from China: A case-control study. Mol Genet Genomic Med. 2019;7(1):e00516.
3. Cohen PA, Jhingran A, Oaknin A, Denny L. Cervical cancer. Lancet. 2019;393(10167):169–182.
4. Jiang C, Li X, Zhao H, Liu H. Long non-coding RNAs: potential new biomarkers for predicting tumor invasion and metastasis. Mol Cancer. 2016;15(1):62.
5. Kazazian K, Go C, Wu H, Brashavitskaya O, Xu R, Dennis JW, et al. Plk4 promotes cancer invasion and metastasis through Arp2/3 complex regulation of the actin cytoskeleton. Cancer Res. 2017 Jan 15;77(2):434–447.
6. Lee RC, Feinbaum RL, Ambros V. The C. elegans heterochronic gene lin-4 encodes small RNAs with antisense complementarity to lin-14J. Cell. 1993;75(5):843–854.
7. Guo R, Gu J, Zhang Z, Wang Y, Gu C. MiR-451 Promotes cell proliferation and metastasis in pancreatic cancer through targeting CAB39. BioMed Res Int. 2017;2017:2381482.
8. Fei H, Chen L, Yong HS Kuerban G. MicroRAN-101 inhibits cell proliferation, invasion, and promotes e-2 in Hela cervical carcinoma cells. Asian Pac J Cancer Prev.

2013;14(10):5915–5920.
9. Chen L, Fei H, Guqun S, Yiming A. MicroRNNA-101 regulates the viability and invasion of cervical cancer cells. Int J Clin Exp Pathol. 2015;8(9):10148–10155.
10. Liang B, Li Y, Wang T. A three miRNAs signature predicts survival in cervical cancer using bioinformatics analysis. Sci Rep. 2017;7(1):5624.
11. Lu HM, Yi WW, Ma YS, Wu W, Yu F, Fan HW, et al. Prognostic implications of decreased microRNA-101-3p expression in patients with non-small cell lung cancer. Oncol Lett. 2018;16(6):7048–7056.
12. Chen L, Long Y, Han Z, Yuan Z, Liu W, Yang F, et al. MicroRNA-101 inhibits cell migration and invasion in bladder cancer via targeting FZD4. Exp Ther Med. 2019;17(2):1476–1485.
13. Zheng HB, Zheng XG, Liu BP. miRNA-101 inhibits ovarian cancer cells proliferation and invasion by down-regulating expression of SOCS-2. Int J Clin Exp Med. 2015;8(11):20263–20270.
14. Biswas S, Kalil K. The microtubule-associated protein Tau mediates the organization of microtubules and their dynamic exploration of actin-rich lamellipodia and filopodia of cortical growth cones. J Neurosci. 2018;38(2):291–307.
15. Svitkina T. The actin cytoskeleton and actin-based motility. Cold Spring Harb Perspect Biol. 2018;10(1):a018267.
16. Tang DD, Gerlach BD. The roles and regulation of the actin cytoskeleton, intermediate filaments and microtubules in smooth muscle cell migration. Respir Res. 2017;18(1):54.
17. Blanchoin L, Boujemaa-Paterski R, Sykes C, Plastino J. Actin dynamics, architecture, and mechanics in cell motility. Physiol Rev. 2014 Jan;94(1):235–63.
18. Del Río-Iñiguez I, Vázquez-Chávez E, Cuche C, Di Bartolo V, Bouchet J, Alcover A. HIV-1 Nef hijacks Lck and Rac1 endosomal traffic to dually modulate signaling-mediated and actin cytoskeleton-mediated T cell functions. J Immunol. 2018;201(9):2624–2640.
19. Tang Y, He Y, Zhang P, Wang J, Fan C, Yang L, et al. LncRNAs regulate the cytoskeleton and related Rho/ROCK signaling in cancer metastasis. Mol Cancer. 2018;17(1):77.
20. Iuliano O, Yoshimura A, Prospéri MT, Martin R, Knölker HJ, Coudrier E. Myosin 1b promotes axon formation by regulating actin wave propagation and growth cone dynamics. J Cell Biol. 2018;217(6):2033–2046.
21. Havrylenko S, Noguera P, Abou-Ghali M, Manzi J, Faqir F, Audrey Lamora A, et al. WAVE binds Ena/VASP for enhanced Arp2/3 complex-based actin assembly. Mol Biol Cell. 2015;26(1):55–65.
22. Swaminathan V, Fischer RS, Waterman CM. The FAK-Arp2/3 interaction promotes leading edge advance and haptosensing by coupling nascent adhesions to lamellipodia actin. Mol Biol Cell. 2016;27(7):1085–1100.

Tables

Table 1
Transwell combined with matrigel test to detect cell invasion ability

project	cells only	miRNA-NC	miRNA-101	*P*
HeLa	128.78 ± 29.06[a]	120.78 ± 23.28[a]	69.67 ± 20.99	0.000
SiHa	333.78 ± 55.92[a]	348.78 ± 52.51[a]	268.78 ± 45.22	0.007
Note (LSD test):Compared with miRNA-101,[a]*P*<0.05 in HeLa group. In SiHa group, [a]*P* < 0.05 compared with miRNA-101.				

Table 2
Scanning electron microscopy to observe the formation of filopodia

project	cells only	miRNA-NC	miRNA-101	*P*
HeLa	61 ± 9[a]	61 ± 11[a]	20 ± 6	0.000
SiHa	46 ± 9[a]	48 ± 7[a]	15 ± 5	0.000
Note LSD test: [a]*P*<0.05 compared with miRNA-101 in the HeLa group. In the SiHa group, [a]*P* < 0.05 compared with miRNA-101.				

Table 3
Comparison of body mass of three groups of subcutaneous xenografts in nude mice

Grouping	Number of cases(mice)	Subcutaneous xenografts in nude body weight(g)
The untransfected group	20	18.47 ± 1.29
The miRNA-NC transfected group	20	18.85 ± 2.38
the miRNA-101 transfected group	20	18.55 ± 1.39
F		0.101
P		0.951

Table 4
Volume comparison of subcutaneous xenografts in three groups of nude mice

Grouping	Number of cases(mice)	volume(mm^3)
the blank group	20	163.51 ± 60.56
the control group	20	159.32 ± 55.83
the experimental group	20	48.27 ± 40.29 [a b]
F		30.162
P		0.000
Note: Compared with the blank group, Pa < 0.05; compared with the control group, Pb < 0.05.		

Table 5
The growth inhibition rates of subcutaneous xenografts(%)

Grouping	the growth inhibition rates(%)
the miRNA-NC transfected group-the non-transfected group	8.49
the miRNA-101 transfected group-the non-transfected group	71.53
the miRNA-101 transfected group-the miRNA-NC transfected group	68.89

Figures

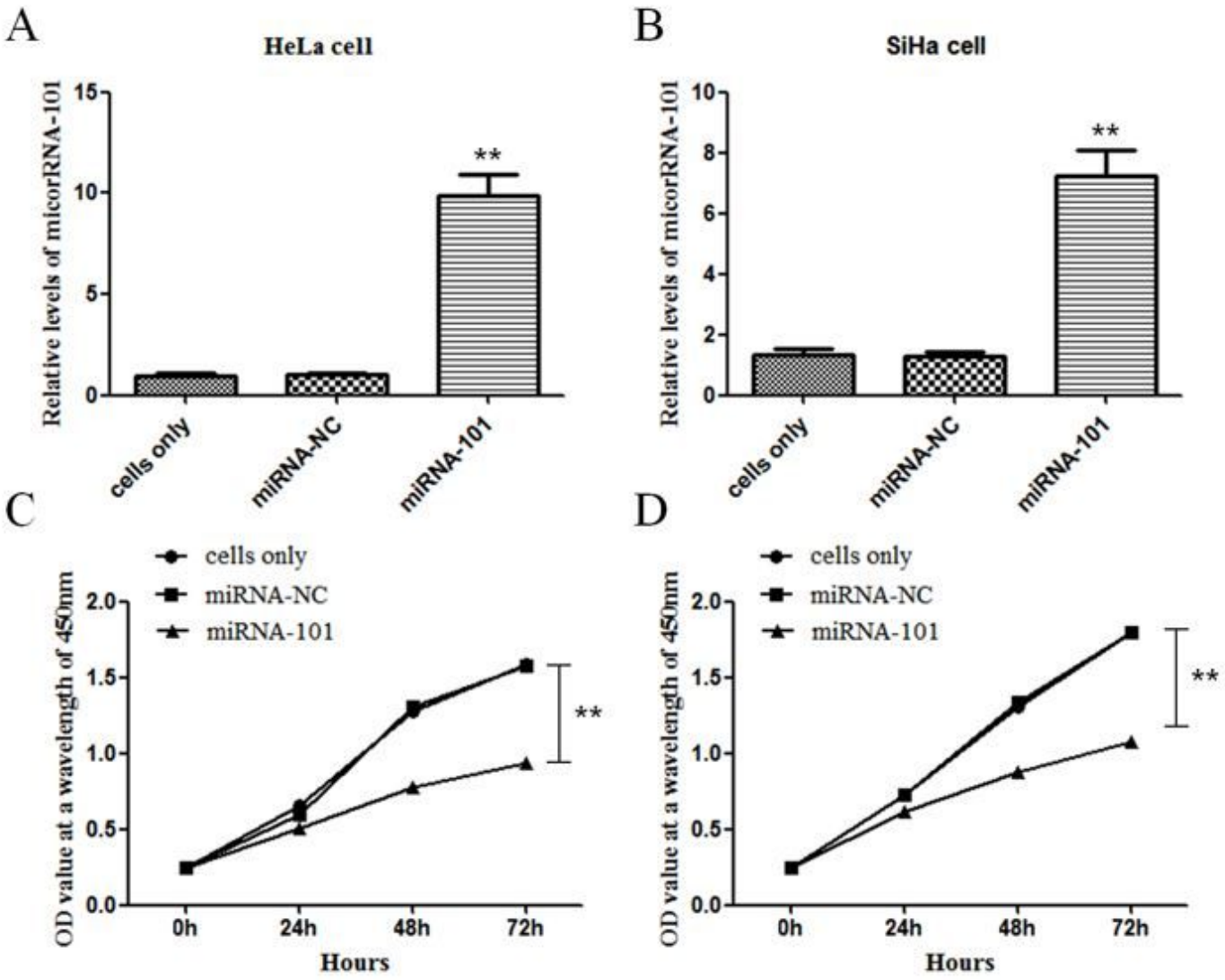

Figure 1

Up-regulation of miRNA-101 significantly inhibited the growth and proliferation of cervical cancer cells. The expression levels of miRNA-101 in HeLa (A) and SiHa(B) cells of the normal control group, the miRNA-NC group, and the miRNA-101 group. The proliferation of cervical cancer HeLa(C) and SiHa(D) cells in the normal control group, the miRNA-NC group and the miRNA-101 group was decreased compared with the normal control group, but no significant difference was found in the miRNA-NC group. * * $P < 0.01$.

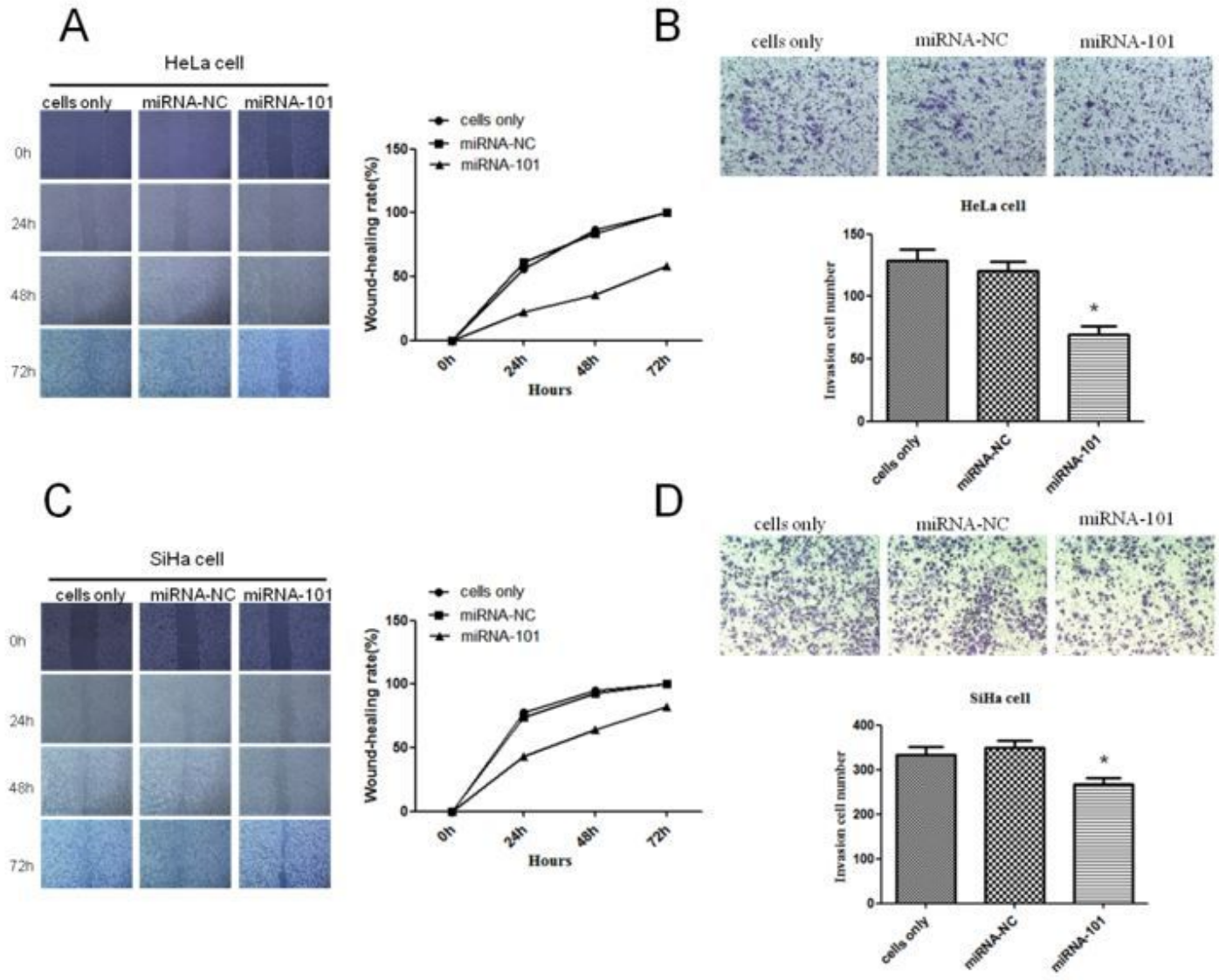

Figure 2

Up-regulation of miRNA-101 significantly inhibited the migration and invasion of cervical cancer cells (A) the wound healing rate of the miRNA-101 overexpression group in HeLa cells was slower than that of the control group. (B) after HeLa cells were transfected with miRNA-NC or miRNA-101 lentivirus, and the invasion of the cells was evaluated by Transwell cell invasion assay. (C) the wound healing rate of the miRNA-101 overexpression group in SiHa cells was slower than that of the control group(D) after transfection of miRNA-NC or miRNA-101 lentivirus into SiHa cells, cell invasion was evaluated by Transwell cell invasion assay. Each experiment was performed at least three times. * P< 0.05, ** P<0.01.

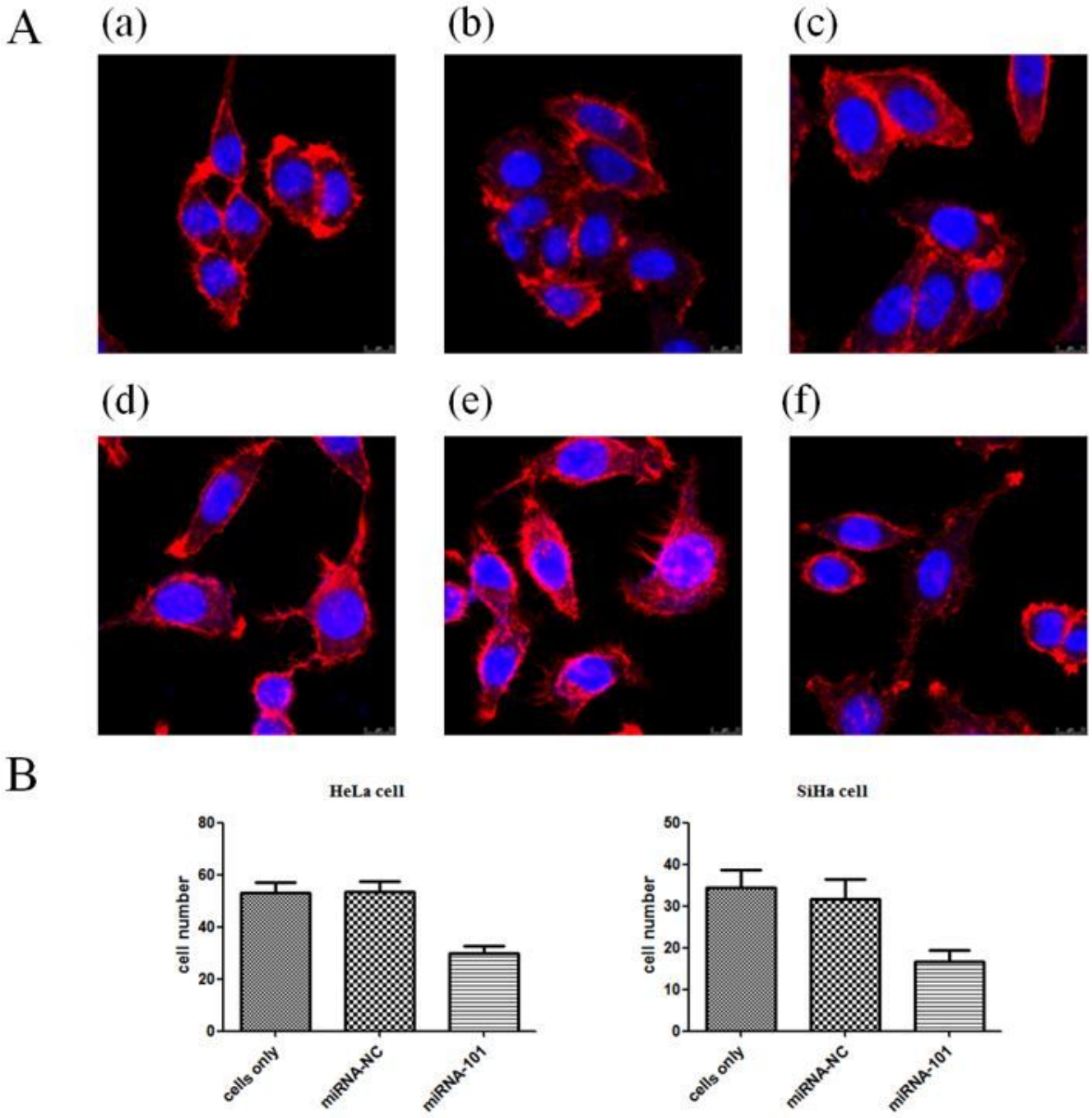

Figure 3

Immunofluorescence and confocal microscopy showed effects of miRNA-101 on the formation of filopodia in cervical cancer cells. (A)confocal microscopy analysis of filopodia with immunofluorescence staining of (a) non-transfected HeLa cells.(b) miRNA-NC transfected HeLa cells.(c)miRNA-101 transfected HeLa cells.(d) non-transfected SiHa cells.(e) miRNA-NC transfected SiHa cells.(f) miRNA-101 transfected SiHa cells. (B)The number of filopodia formed in the miRNA-101 overexpression group were fewer than in the control group in HeLa and SiHa cells.The red fluorescence was rhotamine phalloidin staining and labeling cytoskeletal F-actin. The blue fluorescence was DAPI staining and labeling nuclei.

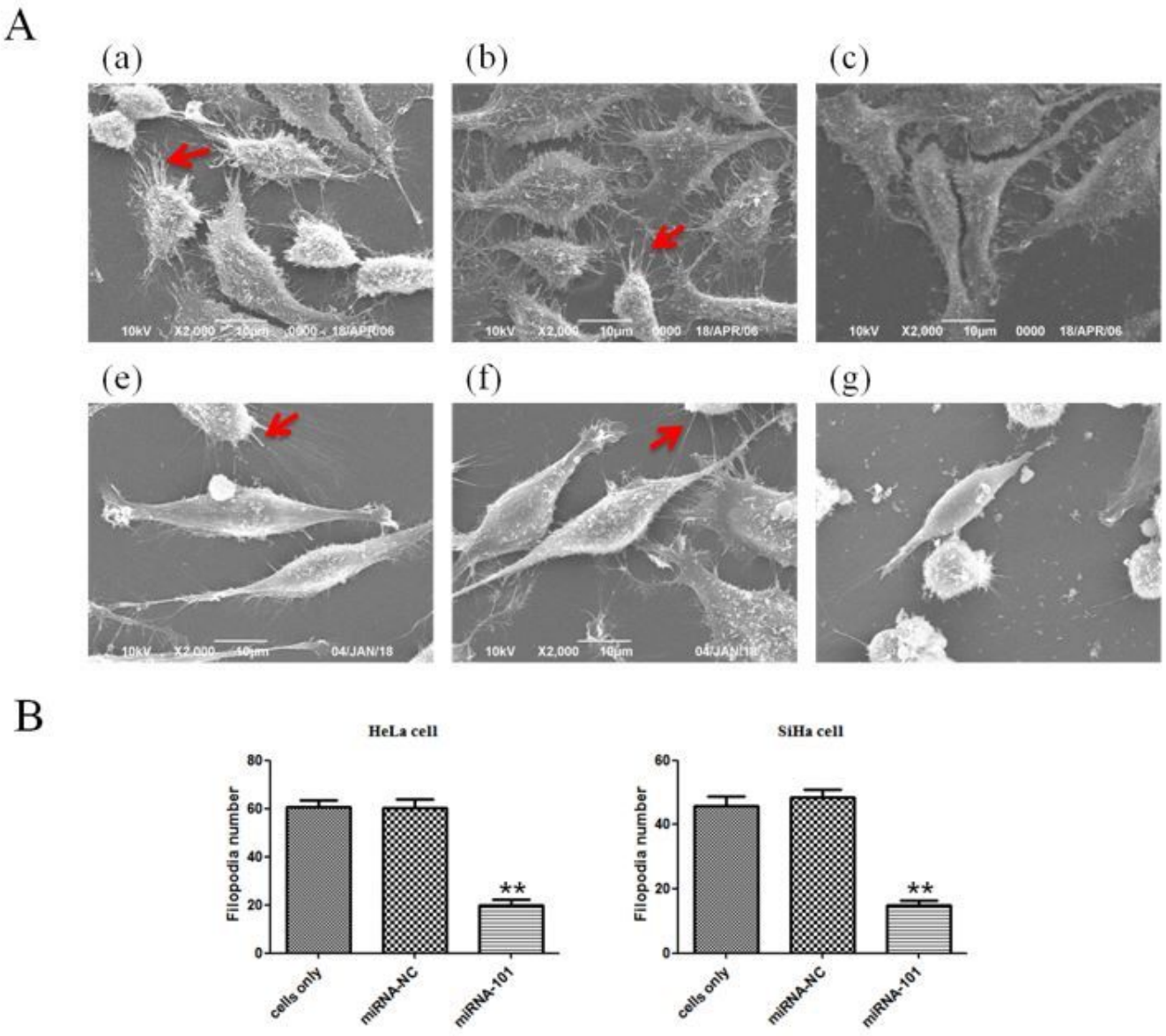

Figure 4

Electron microscope scanning showed the effect of miRNA-101 on the formation of filopodia in cervical cancer cells. (A)Scanning electron micrograph of (a)normal control group of HeLa cells (b)miRNA-NC group of HeLa cells (c)miRNA-101 group of HeLa cells (d)normal control group of SiHa cells (e)miRNA-NC group of SiHa cells (f)miRNA-101 group of SiHa cells. (B)The number of filopodia formed in overexpressing miRNA-101 groups were less than that in control groups in HeLa and SiHa cells.The red arrow represents flopodia.

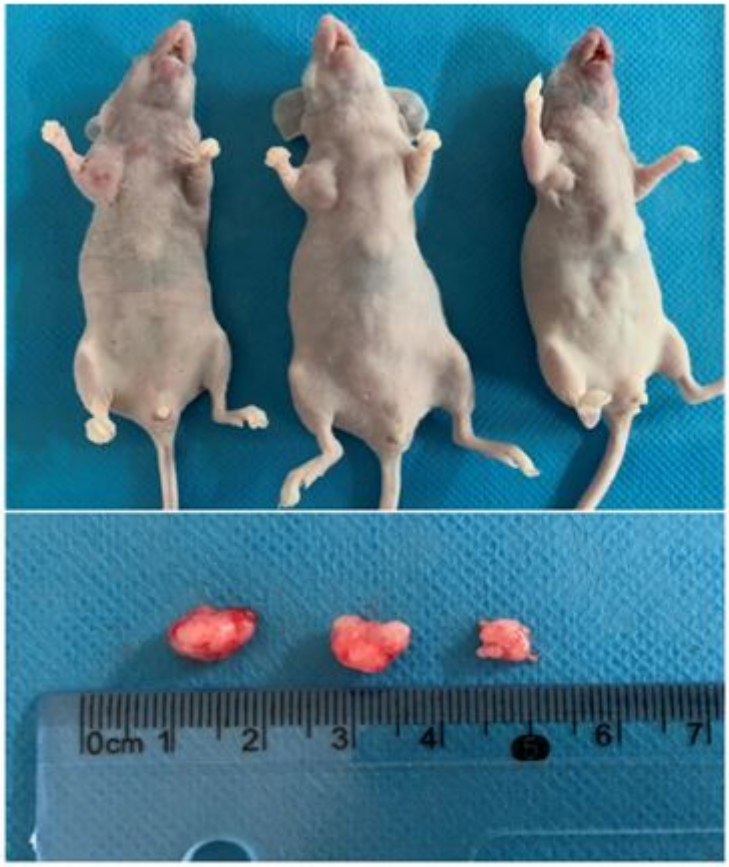

Figure 5

Subcutaneous xenograft nude mice and tumor tissues From left to right in turn is the non- transfected group,miRNA-NC transfected, miRNA-101 transfected group.

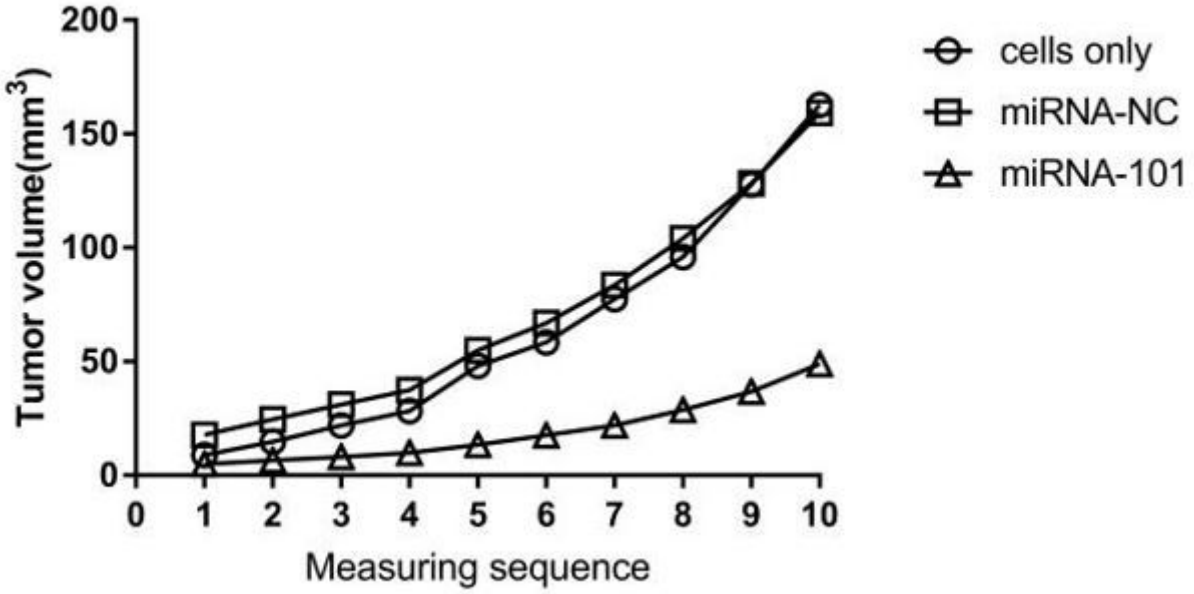

Figure 6

The growth curve of subcutaneous xenografts

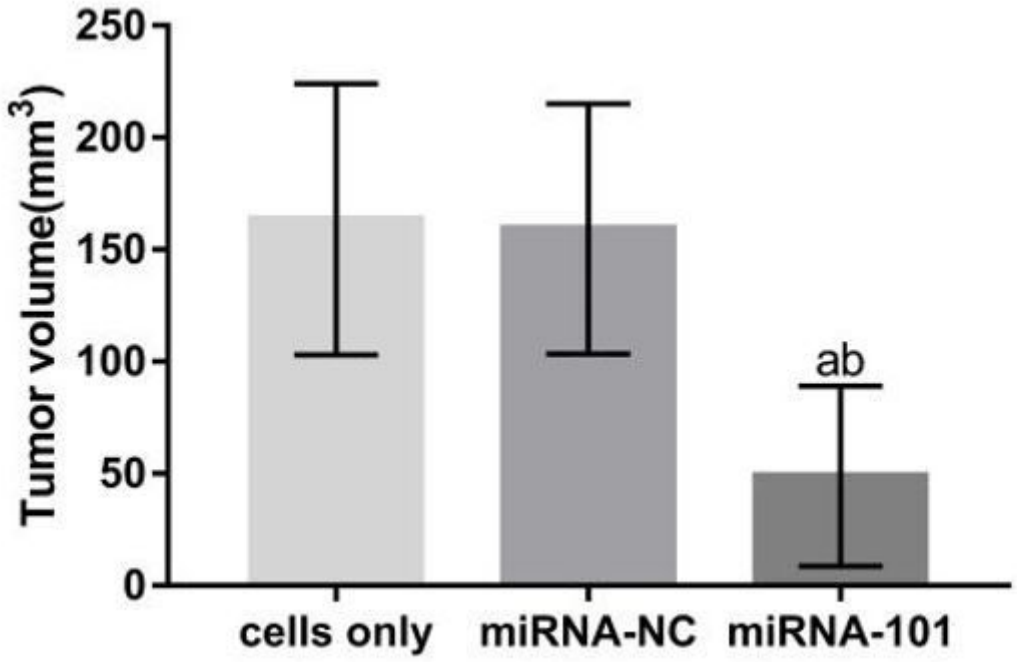

Figure 7

Volume comparison of subcutaneous xenografts in three groups of nude mice

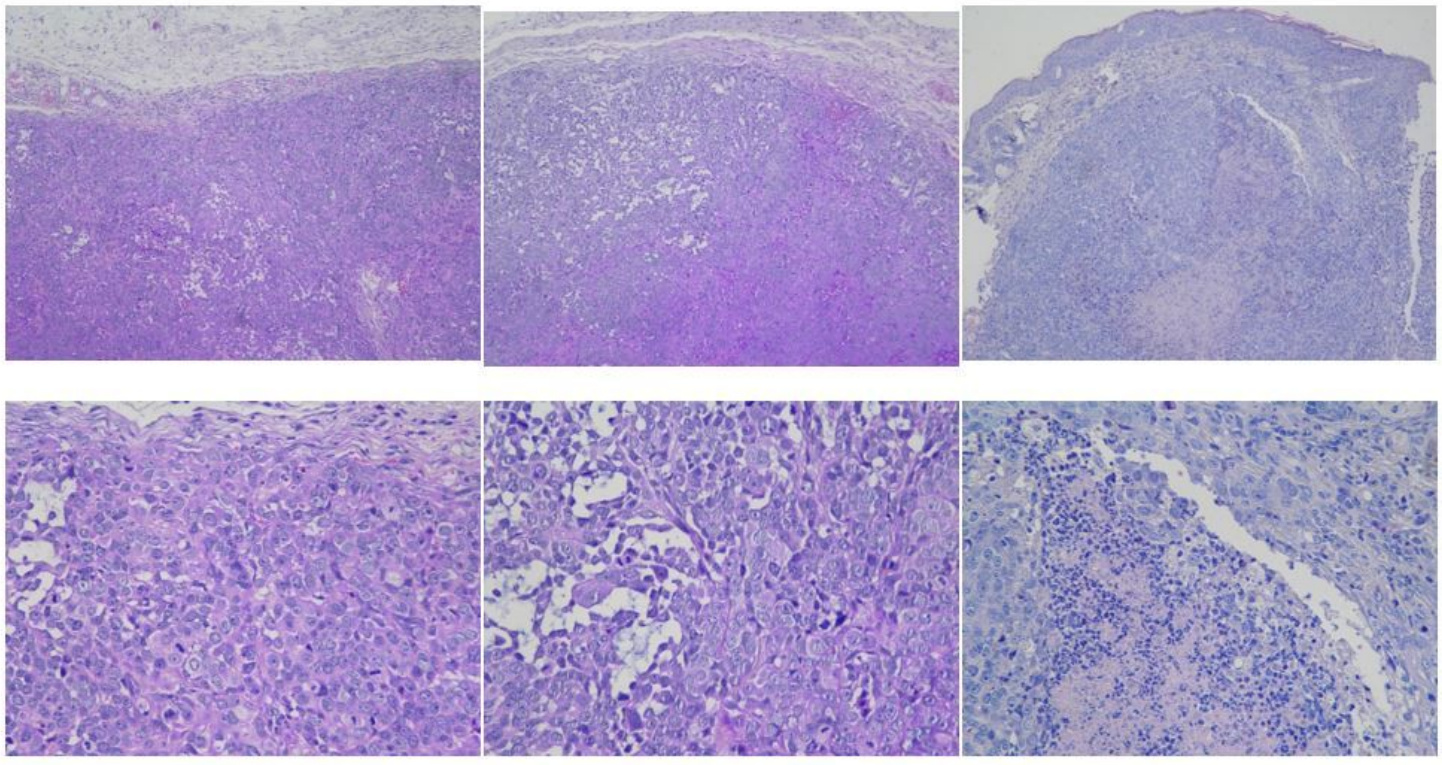

Figure 8

HE staining of subcutaneous xenografts From left to right in turn is the non- transfected group,miRNA-NC transfected, miRNA-101 transfected group. (upper row was x100, lower row was x400)